

## Ultrafast nonthermal terahertz electrodynamics and possible quantum energy transfer in the Nb<sub>3</sub>Sn superconductor

X. Yang,<sup>1</sup> X. Zhao,<sup>1</sup> C. Vaswani,<sup>1</sup> C. Sundahl,<sup>2</sup> B. Song,<sup>1</sup> Y. Yao,<sup>1</sup> D. Cheng,<sup>1</sup> Z. Liu,<sup>1</sup> P. P. Orth,<sup>1</sup> M. Mootz,<sup>3</sup> J. H. Kang,<sup>2</sup> I. E. Perakis,<sup>3</sup> C.-Z. Wang,<sup>1</sup> K.-M. Ho,<sup>1</sup> C. B. Eom,<sup>2</sup> and J. Wang<sup>1,\*</sup>

<sup>1</sup>*Department of Physics and Astronomy and Ames Laboratory, Iowa State University, Ames, Iowa 50011, USA*

<sup>2</sup>*Department of Materials Science and Engineering, University of Wisconsin-Madison, Madison, Wisconsin 53706, USA*

<sup>3</sup>*Department of Physics, University of Alabama at Birmingham, Birmingham, Alabama 35294-1170, USA*



(Received 25 May 2018; revised manuscript received 16 August 2018; published 7 March 2019)

We report terahertz (THz) electrodynamics of a moderately clean A15 superconductor (SC) following ultrafast excitation to manipulate quasiparticle (QP) transport. In the Martensitic normal state, we observe a photo enhancement in the THz conductivity using optical pulses, while the opposite is observed for the THz pump. This demonstrates *wavelength-selective* nonthermal control of conductivity distinct from sample heating. The photo enhancement persists up to an additional critical temperature, above the SC one, from a competing electronic order. In the SC state, the fluence dependence of pair-breaking kinetics together with an analytic model provides an implication for a “one photon to one Cooper pair” nonresonant energy transfer during the 35-fs laser pulse; i.e., the fitted photon energy  $\hbar\omega$  absorption to create QPs set by  $2\Delta_{SC}/\hbar\omega = 0.33\%$ . This is more than one order of magnitude smaller than in previously studied BCS SCs, which we attribute to strong electron-phonon coupling and possible influence of phonon condensation.

DOI: [10.1103/PhysRevB.99.094504](https://doi.org/10.1103/PhysRevB.99.094504)

### I. INTRODUCTION

The competition and interference between SC and other coexisting electronic instabilities appear to be universal in quantum materials. How to exploit the balance of these orders as a control mechanism to achieve ultrafast manipulation of quasiparticle (QP) properties is an outstanding challenge. Answering these questions has been proven important not only in the more sophisticated quantum materials [1–3] but also in some well-established systems such as A15 superconductors [4–9]. Recently, a strikingly long-lived, gapless QP quantum phase with coherent transport is demonstrated by THz quench of a Nb<sub>3</sub>Sn superconducting gap without heating other degrees of freedom [10]. Nb<sub>3</sub>Sn, as a paradigmatic A15 compound, exhibits a Martensitic normal state transition above the superconducting one, which has been ascribed to optical phonon condensation (“dimerization” of Nb atoms) [11], possibly driven by a Van Hove singularity (VHS)–like electronic density of states peaked at  $\sim E_F$  and by strong electron-phonon interaction [5–8,12,13]. The order parameters competing with SC likely exhibit multiple components, both lattice and electronic, e.g., the apparent splitting of the threefold degenerate  $\Gamma_{12}$  band concurrently with an elusive electronic or possibly charge-density-wave (CDW)–like order contribution inferred both from tunneling [9,13,14] and Raman spectroscopy [15].

As a result, the partial Fermi surface gapping,  $\Delta_W \gg \Delta_{SC}$ , associated with the Martensitic anomaly affects the electronic states near  $E_F$  differently from the competing SC order  $\Delta_{SC}$  [7]. This opens an opportunity for exploring ultrafast nonther-

mal manipulation of conductivity via wavelength-selective pumping.

THz spectroscopy is a powerful tool for *quantitative* studies of SC states both in and out of equilibrium. Arising from energy scales in the vicinity of SC gaps  $\Delta_{SC}$  of few meV, terahertz (THz) electrodynamics, characterized by the complex optical conductivity response function  $\tilde{\sigma} = \sigma_1(\omega) + i\sigma_2(\omega)$ , is a direct measure of both dissipation of QPs and inductivity of SC condensate.

Prior THz studies of SC samples mostly revealed “conventional” features in the deep impurity limit,  $\hbar/\tau_{\text{imp}} \gg 2\Delta_{SC}$  [16–18]. In addition, the spectral-temporal dynamics of the order parameters out of equilibrium allow the identification of correlation gaps and co-existing orders. These salient features have not been studied in A15 superconductors and the much-needed comparisons with other BCS SCs are absent, e.g., MgB<sub>2</sub> and NbN without competing orders [16–18].

In this paper, we present THz electrodynamics of Nb<sub>3</sub>Sn following ultrafast optical and THz excitation. Our results show that the nonequilibrium THz conductivity after fs optical pump excitation ( $\sim 1.55$  eV) gains an additional spectral weight that, strikingly, persists far above the superconducting  $T_C$ , while THz pump ( $\sim 4$  meV) shows a reduced THz conductivity. This *wavelength-selective* control of conductivity is not only distinct from sample heating but also goes beyond the conventional picture of ultrafast melting of competing orders.

Furthermore, we observe a rapid, SC pair-breaking process consistent with strong electron-phonon coupling. This, together with an analytic model, provides implications for a quantum limit, energy transfer during  $\sim 35$  fs optical pulses, i.e., one high-energy photon breaks only one low-energy Cooper pair, with the rest of photon energy exciting phonons rather than creating additional QPs. Such “single quanta,”

\*Corresponding author: [jwang@ameslab.gov](mailto:jwang@ameslab.gov)

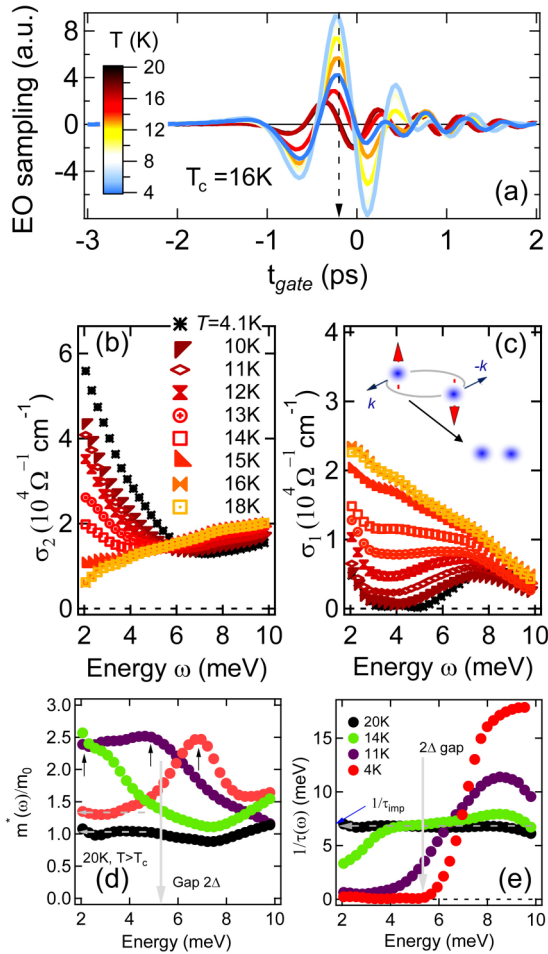


FIG. 1. (a) THz probe transmitted field  $E_{\text{probe}}$  as function of gate delay time  $t_{\text{gate}}$  for the thermal equilibrium state from 4 to 20 K. [(b), (c)] Temperature dependence of imaginary and real parts of the conductivity,  $\sigma_2(\omega)$  and  $\sigma_1(\omega)$ . Inset to (c): Schematic of Cooper pair breaking. (d) Mass renormalization  $m^*(\omega)/m_0$  and (e) momentum scattering rate  $1/\tau(\omega)$  spectra calculated from  $\sigma_2(\omega)$  and  $\sigma_1(\omega)$  in panels (b) and (c). Gray solid line denotes  $2\Delta_{SC}$  gap at 4.1 K. Dashed lines mark the asymptotic  $m^*/m$  and  $1/\tau$  toward zero frequency.

initial transfer of photon energy  $\hbar\omega$  to QPs is determined by  $2\Delta_{SC}/\hbar\omega = 0.33\%$ , a value extracted from fitting 200 fs up to 4 ps pre-bottleneck dynamics.

## II. SAMPLES AND BASIC CHARACTERIZATIONS

A Nb<sub>3</sub>Sn film 20 nm thick was grown by magnetron sputtering on a 1 mm Al<sub>2</sub>O<sub>3</sub> (*R* plane) substrate by cosputtering Nb and Sn at high temperatures.

The ultrafast THz spectroscopy technique is implemented by using three pulses [10,19,20]: optical or THz pump  $E_{op/THz}$ , THz probe  $E_{THz}$  by optical rectification, and optical gating pulse at time  $t_{\text{gate}}$  for electro-optic sampling. The setup was driven by a 1 kHz Ti:sapphire regenerative amplifier with 35 fs duration at 800 nm center wavelength.

The equilibrium time-domain THz transmission field [Fig. 1(a)] and electro-dynamics [Figs. 1(b) and 1(c)] are shown as functions of temperature.

The 4.1 K traces exhibit a diverging  $1/\omega$  response in  $\sigma_2$ , arising from reactive SC condensate, and a dissipationless

conductivity, witnessed in  $\sigma_1$  below  $2\Delta_{SC} = 5.1$  meV. A finite  $\sigma_1$  peak at the lowest frequencies  $<3$  meV originates from intraband absorption of the thermally excited Bogoliubons.

Such conductivity features of SC diminish when approaching  $T_c$ , as seen in the 10 and 15 K measurements shown in Figs. 1(b) and 1(c). As shown in the 16 and 18 K traces, the normal state exhibits a Drude response: a gapless  $\sigma_1(\omega)$  and gradually decreasing  $\sigma_2(\omega)$  toward low frequencies. The relatively narrow linewidth of  $\sigma_1(\omega)$  indicates a much smaller impurity scattering rate,  $\hbar/\tau \sim 7$  meV, than in previous THz studies [16–18]. This also leads to more than two orders of magnitude larger  $l/\xi$  ratio of mean free path over coherence length in our sample, where  $l = v_F\tau = 32$  nm  $\sim 4.5\text{--}8\xi_{\text{exp}}$ , indicative of a moderately clean SC (Supplemental Material [27]).

We now extract the optical self energy  $\Sigma(\omega, T)$  using an extended Drude model [21], which provides information complementary to  $\tilde{\sigma}(\omega)$  and more relevant to characterizing impurity scattering and correlation.

Figures 1(d) and 1(e) present the complex  $\Sigma(\omega, T)$  in terms of the frequency-dependent mass renormalization  $m^*(\omega)/m_0$  and momentum scattering rate  $1/\tau(\omega)$ , which relate to the real and imaginary parts of the  $\Sigma(\omega, T)$ , respectively. We emphasize three key observations in the SC state. First, the  $1/\tau(\omega)$  spectra in Fig. 1(e) clearly reveal a SC gap opening, suppresses the scattering rate below  $2\Delta_{SC}$ , and reduces it to zero at 4.1 K. Second, sharp impurity peaks, commonly seen in dirty-limit SC samples at  $2\Delta_{SC}$  [21], are absent in  $1/\tau(\omega)$  and replaced by a broad cusp in  $m^*(\omega)/m_0$  above  $2\Delta_{SC}$ . Third,  $m^*(\omega)/m_0$  in the SC state as  $\omega \rightarrow 0$  reflects  $n/n_s$ , i.e., the ratio between the electron density  $n$  and the superfluid density  $n_s$ . Here,  $n/n_s(4.1\text{ K}) = m^*(\omega = 0, 4.1\text{ K})/m_0 \sim 1.34$  indicates that  $\sim 75\%$  of the electrons participate in superfluidity, consistent with the superfluid density ratio ( $\sim 70\%$ ) obtained from the optical sum rule  $\int_0^\infty (\sigma_1^n(\omega) - \sigma_1^s(\omega)) d\omega = \frac{\pi}{2} \frac{n_s e^2}{m}$ . This measured  $n_s/n$  is  $\sim 6$  times larger than in superconducting Pb [21].

Next, we simulate the static THz conductivity of Nb<sub>3</sub>Sn by the Mattis-Bardeen (MB) model used for type I, dirty-limit superconductors. It has been used extensively in prior studies [16–18] and successfully accounts for the measured THz electro-dynamics in both NbN and MgB<sub>2</sub> superconductors. Given the normal state conductivity  $\sigma_1(\omega)$  at 16 K, the MB model reproduces the THz response function of Nb<sub>3</sub>Sn at various temperatures plotted in Fig. 2. Simulation results present a clear deviation from experiment data in Figs. 1(b) and 1(c). For example, simulated  $\sigma_2(\omega)$  is much smaller than measured values at 15.5 K, while showing larger divergence at 4 K toward zero frequency. This comparison demonstrates that cleanness of superconductor sample is crucial for accounting the measured THz electro-dynamics in the vicinity of SC gap, which differentiates THz electro-dynamics of cleaner Nb<sub>3</sub>Sn from prior THz results on dirty samples.

## III. ULTRAFAST THZ PROBES OF MARTENSITIC PHASE

Next, we study ultrafast dynamics of the Martensitic normal state in Nb<sub>3</sub>Sn. In Fig. 3(a), we record the photoinduced THz field peak-to-peak amplitude as a function of temperature from 4 to 70 K. The measured raw THz field data is

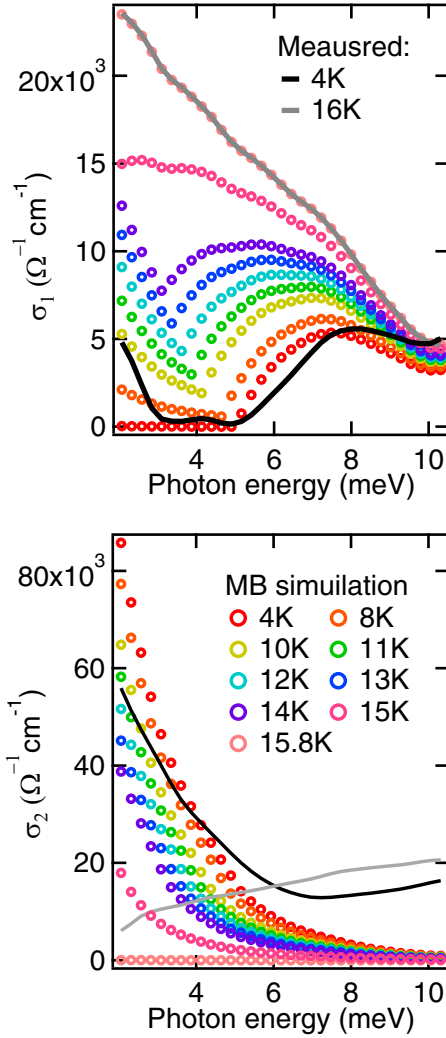


FIG. 2. Temperature-dependent THz conductivity  $\sigma_1(\omega)$  (on top) and  $\sigma_2(\omega)$  (on bottom) at 4K and 16K compared to simulation done by Mattis-Bardeen theory

shown in the time domain in Fig. 3(b) (inset), including the pump-induced change,  $\Delta E(t)$ , at a fixed pump-probe delay  $\Delta\tau_{pp} = 10$  ps (red) and the transmitted field through the unexcited sample,  $E_0(t)$  (gray). Two transitions are visible in Fig. 3(a). As expected for a SC, the photoinduced signal drops significantly at  $T_C \sim 16$  K. Unlike in a conventional SC, however, the signal persists into the normal state and completely vanishes only at a much higher temperature  $T_M \sim 47$  K (inset). Intriguingly, the latter transition in the THz field amplitude coincides with the Martensitic anomaly associated with the structural-electronic instabilities [5–8,11–13]. The inset in Fig. 3(b) reveals such an additional order parameter with a critical temperature  $T_M$ .

The correlation gap  $\Delta_W$  associated with the Martensitic order inferred from scanning tunneling spectroscopy is  $\sim 80$  meV [13] as a CDW-like feature which is out of the spectral window studied here, which makes the Martensitic order relatively “blind” in the low-frequency *equilibrium* conductivity spectra. First, unlike typical density wave orders where a significant spectral weight transfer from low to high frequency develops in conjunction with establishment of the correlation

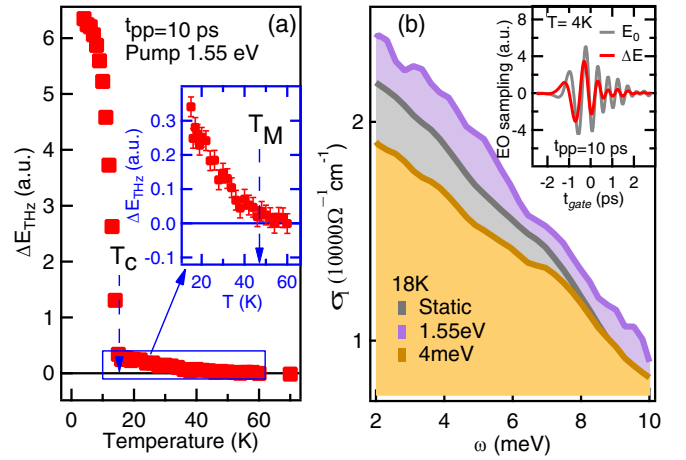


FIG. 3. (a) Temperature dependence of pump-induced change  $\Delta E_{\text{probe}}$  under  $4.02 \mu\text{J}/\text{cm}^2$  excitation fluence.  $\Delta E_{\text{probe}}$  above  $T_C$  is magnified in inset to panel (a), in which Martensitic transition temperature  $T_M = 48$  K is marked by a blue dashed line. (b) Transient state  $\sigma_1(\omega)$  at 10 ps after 1.55 eV (purple), 4 meV (amber) photoexcitation compared to thermal equilibrium (gray) at 18 K. Inset to (b): Transmitted  $E_{\text{probe}}$  through unpumped  $\text{Nb}_3\text{Sn}$  film (gray) and pump-induced change  $\Delta E_{\text{probe}}$  (red).

gap, the Martensitic order represents a very subtle partial gapping of Fermi surface. Our data in Fig. 4 measure this low-frequency conductivity in the normal state  $\text{Nb}_3\text{Sn}$  that allows the determination of a very small spectral weight change in the range of 1–10 meV. Second, temperature dependence of static optical conductivity in  $\text{Nb}_3\text{Sn}$  is affected by two competing effects in the normal state: Increased scattering rate and suppressed Martensitic gap  $\Delta_W$ . As shown in Fig. 4, spectral weight and slope of  $\sigma_1(\omega)$  decrease simultaneously as temperature increases; i.e., scattering rate increase is more significant than spectral weight transfer above SC critical temperature  $T_C$ , which results in a decrease of spectra weight in 1–10 meV by thermal broadening with increasing lattice temperature. It is worth noting that such a decrease of the spectral weight at elevated temperatures is opposite to the strong density wave materials that show an increase of the spectral weight. Such thermal effect makes it difficult to underpin the *nonthermal* suppression of CDW gap from the measured ultrafast conductivity. On the flip side, the above-mentioned issues show that the pump-probe measurement in Fig. 3 with superior

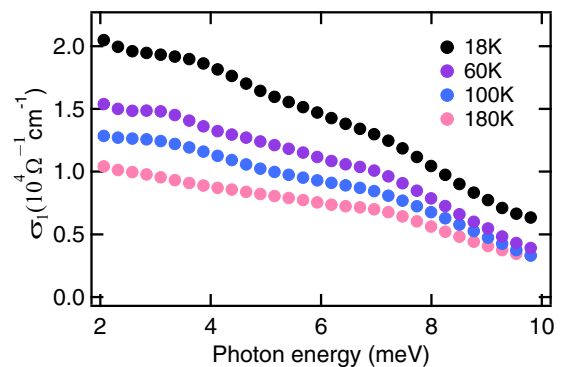


FIG. 4. Normal-state static THz conductivity  $\sigma_1(\omega)$  at temperatures from 18 to 180 K.

signal-noise ratio represent a powerful method to probe the subtle change of Martensitic phase with a clear transition temperature at 47 K. The pump-induced increase of spectral weight indicates a distinct nonthermal ultrafast softening of the correlation gap since laser-induced heating will decrease the spectra weight after the pump. Therefore, this demonstrates the clear ultrafast measurement of the Martensitic order and nonthermal melting of its correlation gap.

Next we also demonstrate *wavelength-selective* nonthermal control of conductivity in Nb<sub>3</sub>Sn below. The competing  $T_M$  order above SC allows such control by tuning the pump between the optical and THz frequency range above or below the correlation gap  $\Delta_W$ . We start with the normal state at 18 K slightly above  $T_C$ . The nonequilibrium  $\sigma_1(\omega)$  data are shown in Fig. 3(b) for 1.55 eV (optical, purple) and 4 meV (THz, yellow) pump photon energy. After 1.55 eV pump excitation (black), the low-frequency conductivity  $\sigma_1(\omega)$  gains an additional spectral weight over its equilibrium (no pump) values (gray), which is responsible for the nonvanishing, pump-induced signals  $\Delta E_{THz}$  in the normal state below  $T_M$  shown in Fig. 3(a). This pump-induced enhancement is consistent with nonthermal softening of the correlation gap that develops at the  $T_M$  transition from  $\Gamma_{12}$  phonon condensation (dimerization) and/or electronic VHSs, by optical excitation with  $\hbar\omega_{op} \gg \Delta_W$ . Such softening gives rise to spectral weight transfer to the Fermi surface from high energies above  $\Delta_W$ . Note that laser-induced heating will only decrease the THz spectral weight after the pump in Nb<sub>3</sub>Sn, as shown in Fig. 3. The absence of spectral weight increase by thermal broadening in the Martensitic normal state results from very subtle partial gapping of the Fermi surface, opposite to typical CDW materials. Most intriguingly, by changing the pump photon energy to 4 meV, i.e.,  $\hbar\omega_{THz} \ll \Delta_W$ , we observe pump-reduced (purple) instead of pump-enhanced conductivity (brown), shown in Fig. 3(b). This opposite behavior indicates that photoexcitation at sufficiently low frequencies fails to strongly quench the  $\Delta_W$  gap and, instead, depletes the Fermi sea portion with a nonthermal, threshold behavior [10,22].

In all cases, the observed pump-wavelength-dependent behavior represents a direct evidence for ultrafast nonthermal control of the THz conductivity by tuning pump photoexcitation above (correlation gap melting) and below (Fermi sea partial depletion)  $\Delta_W$ . Note that the unusual pump wavelength dependence is absent in previously studied CDW/SDW materials [2,3,23] and BCS SCs without coexisting orders [16–18]. The distinct nonthermal photoexcitation control of QP conductivity provides evidence for an additional electronic instability associated with the Martensitic anomaly beyond the conventional structural one.

#### IV. “ONE-PHOTON–ONE-COOPER-PAIR” QUANTUM ENERGY TRANSFER DURING THE LASER PULSE $\sim 30$ FS

We turn to the nonequilibrium Cooper pair breaking (CPB) responses in the superconducting state after fs optical excitation. For  $\hbar\omega_{op} \gg 2\Delta_{SC}$ , CPB processes can be driven by multiple interactions between the condensate and photoexcited QPs or high-frequency phonons (HFPs).

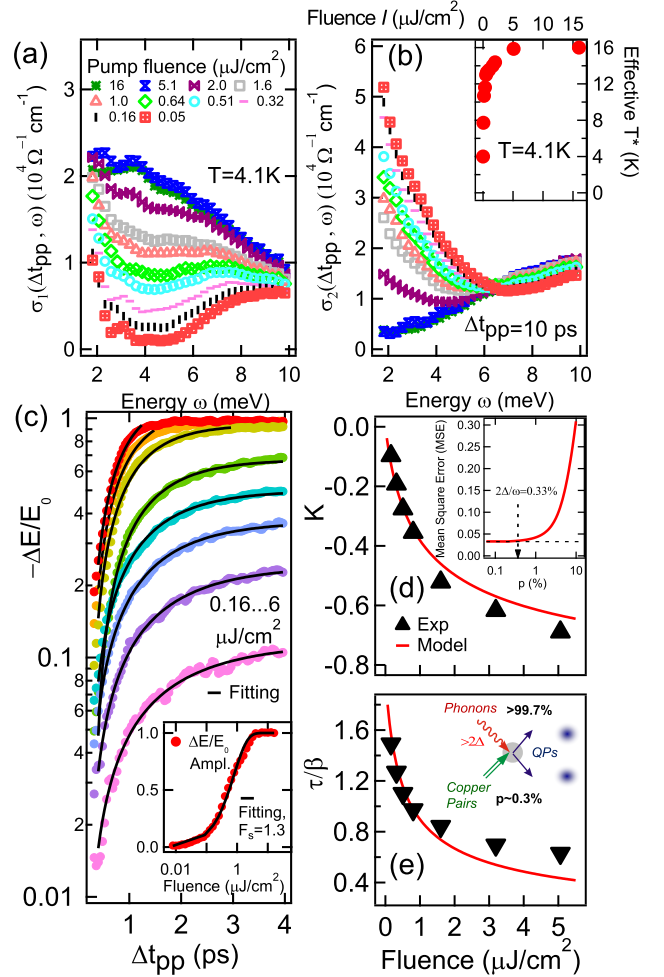


FIG. 5. [(a), (b)] Post-pump conductivity  $\sigma_1(\omega)$  and  $\sigma_2(\omega)$  at  $t_{pp} = 10$  ps under  $0.05$ – $16 \mu\text{J}/\text{cm}^2$  pumping fluence. Inset to panel (b) shows effective temperature  $T^*$  at various fluences. (c) Pump-probe dynamics  $\Delta E/E$  measured in experiment (colored dots) are fitted by RT model (black lines). Inset to panel (c) shows the fitting results of  $\Delta E/E$  at  $t_{pp} = 10$  ps, 4 K by saturation curve  $[1 - \exp(-I/F_s)]$ , in which  $I$  is the pumping fluence and  $F_s = 1.3 \mu\text{J}/\text{cm}^2$ . [(d), (e)] Fluence-dependent parameters  $K$  and  $\tau/\beta$  (black triangle) are fitted by  $\Omega$  and fluence-independent  $\{R, \beta, p\}$  (red line). Inset to panel (d): Mean square error (MSE) of  $\{R, \beta\}$  by varying  $p$ . Inset to panel (e) shows the microscopic CPB process.

Previous works have shown that majority of the absorbed photon energy subsequently transfers to the phonon reservoir during the fs excitation, which continues to break Cooper pairs [16,17]. Figures 5(a) and 5(b) plot the nonequilibrium THz conductivity  $\sigma_1(\omega)$  and  $\sigma_2(\omega)$  of Nb<sub>3</sub>Sn, for various fluences of 1.55 eV pump photoexcitation at  $T = 4.1$  K. We observe very similar spectral shapes to those seen at various temperatures in equilibrium (Fig. 1). Photoinduced QPs gradually close the SC gap  $2\Delta_{SC}$ . At the same time, the low-frequency  $1/\omega$  divergence in  $\sigma_2$  diminishes with increasing pump fluence  $I_{\text{pump}}$ . SC features disappear simultaneously above  $4 \mu\text{J}/\text{cm}^2$ . The thermalized gap  $\Delta_{SC}(I_{\text{pump}})$  and the superfluid density  $n_s$ , readily seen from transient THz spectra, quickly diminish as  $I_{\text{pump}}$  approaches the same

fluence. An elevated electron/lattice transient temperature  $T^*$  established after the pump can be extracted by fitting the conductivity data. As shown in the inset of Fig. 5(b),  $T^* \rightarrow T_c$  is clearly visible at the quenching fluence  $\sim 4 \mu\text{J}/\text{cm}^2$ . Therefore, conductivity at  $\Delta t_{pp} = 10$  ps for  $T < T_c$  is consistent with previous  $T^*$  model of nonequilibrium superconductivity [21,24,25].

We track the early-time, pair-breaking dynamics prior to the establishment of a  $T^*$  quasiequilibrium temperature regime due to scattering of condensate with HFPs and hot QPs.

The experimentally observed ultrafast THz signals for various pump fluences, which reflect the photoexcited QP density  $n(t)$ , are presented in Fig. 4(c). They show faster CPB with increasing pump fluence during the first 4 ps. In order to reveal the microscopic energy transfer among various reservoirs, we model the CPB kinetics based on the widely used Rothwarf-Taylor (RT) model [26] that is extensively discussed in Ref. [25]. This model is expected to be valid at latter up to 4 ps timescales following the ‘‘initial condition’’ created during the very early 10 fs range regime of ultrafast dynamics dominated by electron-phonon coherences and by quasiparticle and phonon nonthermal populations created during the laser pulse. The dynamics after this initial regime is characterized by QP and HFP densities,  $n(t)$  and  $N(t)$ , described by two coupled differential equations [16,17,25,26]. The rise of  $n(t)$  in time originates from the prebottleneck, CPB process preceding the QP relaxation, which can be described by the analytical expression [25]

$$n(t) = \frac{\beta}{R} \left[ -\frac{1}{4} - \frac{1}{2\tau} + \frac{1}{\tau} \frac{1}{1 - K \exp(-t\beta/\tau)} \right], \quad (1)$$

where  $K$  and  $\tau$  are dimensionless parameters determined by the initial conditions:  $K = [(\tau/2)/(4Rn_0/\beta + 1) - 1]/[(\tau/2)/(4Rn_0/\beta + 1) + 1]$  and  $\frac{1}{\tau} = \sqrt{1/4 + 2R/\beta(n_0 + 2N_0)}$ . Here,  $\beta$  is the CPB probability by absorption of HFP and  $R$  is the bare QP bimolecular decay rate.  $n_0$  and  $N_0$  are the initial QP and HFP densities immediately after 35 fs photoexcitation.  $\beta$  and  $R$  are fluence-independent parameters under weak excitation limit, when  $n_0$  is much smaller than the material-dependent value  $\beta/R$ . Figure 5(c) presents the best fits, which show very good agreement with the data. The fitting parameters  $\tau/\beta$  and  $K$  are extracted as the function of fluence and plotted in Figs. 5(d) and 5(e) respectively.

Further quantitative information can be obtained by fitting  $\tau/\beta$  and  $K$  versus the absorbed energy density  $\Omega$ . Here  $\Omega$  at  $I_q = 4.02 \mu\text{J}/\text{cm}^2$  is equal to the SC condensate energy  $U = 4757 \text{ mJ}/\text{mol}$  [23]. The determination of  $\Omega$  is critical for this purpose, which has been described in details in the Supplementary Material [27]. Given the lack of direct information about the very early 10 fs range quantum regime during the laser pulse, we treat the initial condition phenomenologically, which can be extracted from the measured dynamics  $\geq 250$  fs and a rigorous error analysis. Denoting the portion of the absorbed energy that initially goes into QP excitation as  $p$ , we have  $n_0 = p\Omega/\Delta$  and  $N_0 = (1 - p)\Omega/2\Delta$  created by 35 fs photoexcitation. The best fit to the extracted  $\tau/\beta$  and  $K$  data, obtained by minimizing the mean-square error (MSE) of

the parameter set  $\{p, R, \beta\}$ , is achieved for  $p = 0.2 \pm 0.1\%$ , which gives the values of  $\beta^{-1} = 1.0 \pm 0.1 \text{ ps}$  and  $R = 105.5 \pm 10 \text{ ps}^{-1} \text{ unit cell}^{-1}$ . We further plot the MSE of the above fitting as function of  $p$  in Fig. 4(d) by only fitting  $\{R, \beta\}$  for each fixed  $p$  (Supplemental Material [27]). The further fitting details are described in the Supplemental Material [27]. Intriguingly, a strong deviation from the minimum error starts at a very small  $p \sim 0.33\%$  that coincides with  $2\Delta_{SC}/\hbar\omega$ , as marked (dashed arrow) in Fig. 5(d). The fitted 0.33% value implies a quantum limit of the energy-transfer process during 35 fs photoexcitation of the A15 system, i.e., one high-energy photon,  $\hbar\omega = 1.55 \text{ eV}$ , breaks only one pair,  $2\Delta_{SC} = 5.1 \text{ meV}$ , with simultaneous excitation of phonon populations during initial QP cascading [inset, Fig. 5(e)]. Although a direct measurement of the 10 fs transient state is technically challenging to resolve, this conclusion is consistent with much faster CPB dynamics in  $\text{Nb}_3\text{Sn}$ , as shown in Fig. 5(c), for the first 100 fs. Pump-probe signal saturates within 4 ps even at lowest fluence, corresponding to 10% of total Cooper pair breaking. In comparison, under a similar pumping condition, it takes tens and even hundreds of ps for  $\text{NbN}$  and  $\text{MgB}_2$  to reach the same condition and maximum of pump-probe signals [16,17]. Applying the same standard fitting and error analysis leads to at least one order of magnitude lower initial energy transfer in  $\text{Nb}_3\text{Sn}$  than any previously measured BCS SCs: 0.33% here vs  $\text{MgB}_2$  ( $p \sim 6\%$ ) [16] and  $\text{NbN}$  ( $p \sim 9\%$ ) [17].

The possible quantum energy transfer process is consistent with strong electron-phonon couplings in A15 SCs. The value of electron-phonon coupling constant  $\lambda$  can be determined from the relation  $R = \frac{8\pi v \lambda \Delta_{SC}^2}{\hbar N(0) \omega_D^3}$ . Here  $\omega_D$  is the phonon cutoff frequency,  $N(0)$  is the electronic density of states per unit cell at the Fermi level, and  $v$  is the number of atoms per unit cell. We obtain  $\lambda \approx 2.0$ , which agrees very well with previous estimates of  $\lambda \approx 1.8 \pm 0.15$  [28] and is two times larger than in the previously studied  $\text{NbN}$ . In addition, a much higher phonon-pair scattering probability  $\beta \sim 1 \text{ ps}^{-1}$  is seen in  $\text{Nb}_3\text{Sn}$  as compared to  $\text{MgB}_2$  ( $\beta = 1/15 \text{ ps}^{-1}$ ) [16] and  $\text{NbN}$  ( $\beta = 1/6 \text{ ps}^{-1}$ ) [17]. Here, phonon condensation from Martensitic order already is a part of the SC electronic order which can potentially be much more efficiently excited during the pulse that differentiates the A15 from other SCs.

## V. DISCUSSIONS ON MODEL ANALYSIS AND ENERGY TRANSFER

The Cooper pair breaking (CPB) dynamics of high-energy photons can be quantitatively analyzed using the RT model, which has been applied to  $\text{NbN}$  [17] and  $\text{MgB}_2$  [16] superconductors. Prior experimental studies are summarized in Table I and compared to our work. The fitting procedure is described below.

To understand the difference in the fitted values of  $\beta$  (i.e., CPB probability by adsorption of HFP) and  $R$  (i.e., bare QP recombination rate) in different systems, we further computed  $\beta/R$  in  $\text{MgB}_2$ ,  $\text{NbN}$ , and  $\text{Nb}_3\text{Sn}$  as it has the dimensionality of concentration and can be expressed in terms of material intrinsic properties:

$$\frac{\beta}{R} = \frac{N(0)^2 \pi \omega_D^3}{18\nu\Delta}, \quad (2)$$

TABLE I. Comparison of optical pump–THz probe experiment on NbN, MgB<sub>2</sub>, and Nb<sub>3</sub>Sn superconductor.

	NbN [17]	MgB <sub>2</sub> [16]	Nb <sub>3</sub> Sn
Transport lifetime	246 cm <sup>-1</sup> = 22 fs	37 meV = 18 fs	8.27 meV = 80 fs
Photoexcitation pulse duration	50fs	150fs	35fs
Electron-phonon coupling $\lambda$	1.1	0.7-0.9	2
$p$	~9%	~6%	~0.33%

where  $N(0)$  is the electronic density of states (DOS) per unit cell,  $\omega_D$  is the Debye energy,  $\nu$  is the number of atoms per unit cell, and  $\Delta$  is the superconducting gap.

The calculated results and other key parameters of different materials (NbN, MgB<sub>2</sub>, and Nb<sub>3</sub>Sn) are summarized in Table II. Fitted  $\beta/R$  shows a decent agreement with calculated values by Eq. (10). We found that  $\beta/R$  in Nb<sub>3</sub>Sn is more than 10 times higher than the other two systems, which is attributed to the much larger DOS at the Fermi level. The different fitting parameters for Nb<sub>3</sub>Sn can be readily observed in pump-probe traces. After 35 fs photoexcitation, Nb<sub>3</sub>Sn reaches the saturation QPs density in a much shorter time than NbN and MgB<sub>2</sub>. Quantitatively, at optical fluence corresponding to 10% pair breaking, Nb<sub>3</sub>Sn takes 4 ps to reach the peak of QPs density, an order of magnitude faster than NbN (20 ps) [17] and MgB<sub>2</sub> (40 ps) [16]. Such behavior is consistent with the much larger pair breaking probability  $\beta$  in Nb<sub>3</sub>Sn from fitting.

The above fitting results is obtained under the condition  $\Omega \sim U_{BCS}$ . Varying  $\Omega$  only changes value of  $R$  without affecting the other two fitting parameters,  $p = 0.2\%$  and  $\beta = 1.0$ . Assuming that the optical energy absorption is  $\Omega \sim 10U_{BCS}$ , this will give  $R \sim 10.5$  and produces unphysical result for  $\beta/R \sim 0.095$ , contradicting Eq. (10). Therefore, this cannot be the correct scenario for Nb<sub>3</sub>Sn. On the other hand,  $\beta/R$  shows a very good agreement with Eq. (10) for NbN and MgB<sub>2</sub>, when 800-nm energy absorption matches well with BCS condensation energy. Further discussion about fitting parameters are described in Supplemental Material [27].

The nonequilibrium Cooper pair breaking responses in the superconducting state after 35 fs optical excitation can be roughly divided into several temporally overlapping stages. First, quantum nonthermal regime during the optical pulse photoexcitation less than 35 fs. This initial temporal regime is not directly resolved experimentally here, but sets up the

initial condition for the ps dynamics that is directly observed in the present experiment (Fig. 5). There is no microscopic theory yet to fully account for this initial regime, which in our A15 system involves coherence and nonthermal populations of both electrons and phonons. The optical phonon condensation in the SC ground state below the Martensitic transition temperature is perturbed by the photoexcitation process, leading to photoinduced electron-phonon dynamics. Since femtosecond pulses are shorter than the characteristic timescales of nonthermal SC dynamics, we have chosen a phenomenological approach based on the standard Rothwarf-Taylor model. The portion of absorbed energy  $p$  initially goes into QP excitations without lattice excitation while the rest excites phonon populations both during and after pair breaking. We thus characterize phenomenologically the initial condition that triggers subsequently the incoherent dynamics after the pulse. Second, the prebottleneck regime accounts for the formation dynamics of the phonon bottleneck. Here, the CPB kinetics can be also based on the Rothwarf-Taylor model, which has been extensively and successfully applied in various SC systems and can be derived microscopically within a Markovian quasiadiabatic approximation. Previous works have shown that the majority of the absorbed photon energy subsequently transfers to the phonon reservoir as high-frequency phonons and then continues to break Cooper pairs after the photoexcitations, as shown in Tables I and II. Third, bottleneck recovery regime takes place at very long ( $\sim 100$  ps) timescales. The first two regimes are the focus in this paper.

We emphasize three points. First, what we have observed here, based on evidence extracted from the high-quality data and exact analysis, is that although the 10 fs regime is not directly accessed in our and other experiments, it is still possible to determine  $p$  from high signal-to-noise-ratio data obtained during the longer, 200 fs to 4 ps prebottleneck time regime.

TABLE II. Comparison of the key parameters among NbN, MgB<sub>2</sub>, and Nb<sub>3</sub>Sn superconductor.

	MgB <sub>2</sub> [16]	NbN [17]	Nb <sub>3</sub> Sn
$T_c$	~39 K	~15 K	~16 K
$\lambda$	0.7–0.9	1–1.2	1.8 ± 0.15
SC gap $\Delta$	$\Delta_1 = 2.2$ meV $\Delta_2 = 7.2$ meV at 4.2 K	$\Delta = 3.07$ meV	$\Delta = 2.55$ meV
$N(0)$ (spin cell eV) <sup>-1</sup>	0.7	0.88	11.4
$\omega_D$	0.064 eV (750 K)	0.31 eV (363 K)	0.02 eV (230 K)
$p$	6%	9%	~0.3%
$R$ (ps <sup>-1</sup> unit cell <sup>-1</sup> )	100 ± 30	160 ± 20	105 ± 10
$\beta$ (ps <sup>-1</sup> )	1/(15 ± 2)	1/(6 ± 1)	0.99
Rising time	~40 ps	~20 ps	~4 ps
$\beta/R$ from fitting (unit cell <sup>-1</sup> )	0.00067	0.001	0.0095
$\beta/R$ from Eq. (10) (unit cell <sup>-1</sup> )	0.001	0.0007	0.0089

In our case, the extracted initial energy transfer is 0.33%, the same as  $2\Delta/(\hbar\omega)$  determined by SC gap and photoexcitation energy. Thus, one high-energy photon  $\hbar\omega$  basically breaks one low-energy Cooper pair  $2\Delta$  during the coherent excitations of optical pulse of 30 fs (the quantum SC quench regime) accompanied by phonon excitation. We refer the observation of one-photon-to-one-pair, nonresonant energy transfer during the fs optical excitations as quantum energy transfer. Second,  $p$  in Nb<sub>3</sub>Sn is two orders of magnitude smaller than in NbN and MgB<sub>2</sub>, as shown in Table II, which provides the much needed comparisons between these samples. Third, our data indicate that phonon emission is much more efficient during the QP decoherence and population buildup immediately after and during the pulse  $\sim 30$  fs. This is consistent with enhanced  $e$ -phonon coupling in Nb<sub>3</sub>Sn and the optical phonon condensation in the ground state below the Martensitic transition that differentiates A15 from other simpler SCs. Note, however, that the exact microscopic dynamics of quantum quench of superconductivity and buildup of the QP population immediately after fs pulse is still lacking, which warrants further study for the development of the nonequilibrium quantum quench dynamics of a strongly coupled  $e$ -lattice system with optical phonon condensation in the ground state.

## VI. CONCLUSION

In summary, we demonstrate ultrafast nonthermal control of the THz conductivity in the Martensitic normal state by

tuning the pump photon energy and identify a competing electronic order in the normal state below the Martensitic anomaly in Nb<sub>3</sub>Sn. In the SC state, we reveal a possible quantum energy transfer during the initial quantum nonthermal regime, which we attribute to strong electron-phonon coupling and optical phonon condensation in the ground state. The distinct ultrafast THz electrodynamics of the model A15 compound with electron-phonon complex order offers perspectives to probe the very early,  $\sim 10$  fs pair-breaking dynamics in unconventional superconductors [29] and to manipulate other competing order systems such as magnetic materials [30–32].

## ACKNOWLEDGMENTS

Work at Iowa State University was supported by the Army Research Office under Award No. W911NF-15-1-0135 (THz spectroscopy). The theoretical work was supported by the Ames Laboratory, U.S. Department of Energy, Office of Science, Basic Energy Sciences, Materials Science and Engineering Division, under Contract No. DE-AC02-07CH11358 (theoretical modeling and numerical simulations). The THz instrument was supported in part by the Keck Foundation (J.W.). Work at Wisconsin (sample growth and basic characterizations) was supported by the DOE Office of Basic Energy Sciences under Award No. DE-FG02-06ER46327. The extra analysis done at the University of Alabama, Birmingham, was supported by the U.S. Department of Energy under Contract No. DE-SC0019137 (M.M. and I.E.P.).

- 
- [1] T. Li, A. Patz, L. Mouchliadis, J. Yan, T. A. Lograsso, I. E. Perakis, and J. Wang, *Nature (London)* **496**, 69 (2013).
  - [2] A. Patz, T. Li, S. Ran, R. M. Fernandes, J. Schmalian, S. L. Bud'ko, P. C. Canfield, I. E. Perakis, J. Wang *et al.*, *Nat. Commun.* **5**, 3229 (2014).
  - [3] M. Porer, U. Leierseder, J. M. Ménard, H. Dachraoui, L. Mouchliadis, I. E. Perakis, U. Heinzmann, J. Demsar, K. Rossnagel, and R. Huber, *Nat. Mater.* **13**, 857 (2014).
  - [4] M. Kataoka, *J. Phys. C* **19**, 2939 (1986).
  - [5] R. N. Bhatt, *Phys. Rev. B* **16**, 1915 (1977).
  - [6] S. H. Muller, G. M. Tuynman, E. G. Sieverts, and C. A. J. Ammerlaan, *Phys. Rev. B* **25**, 25 (1982).
  - [7] G. Bilbro and W. L. McMillan, *Phys. Rev. B* **14**, 1887 (1976).
  - [8] B. Sadigh and V. Ozolinš, *Phys. Rev. B* **57**, 2793 (1998).
  - [9] J. K. Freericks, A. Y. Liu, A. Quandt, and J. Geerk, *Phys. Rev. B* **65**, 224510 (2002).
  - [10] X. Yang, C. Vaswani, C. Sundahl, M. Mootz, P. Gagel, L. Luo, J. H. Kang, P. P. Orth, I. E. Perakis, C. B. Eom, and J. Wang, *Nat. Mater.* **17**, 586 (2018).
  - [11] G. Shirane and J. D. Axe, *Phys. Rev. B* **4**, 2957 (1971).
  - [12] R. S. Markiewicz, *J. Phys. Chem. Solids* **58**, 1179 (1997).
  - [13] R. Escudero and F. Morale, *Solid State Commun.* **150**, 715 (2010).
  - [14] T. Ekino, A. M. Gabovich, A. Sugimoto, Y. Sakai, and J. Akimitsu, in *Superconductors-New Developments*, edited by A. Gabovich, IntechOpen Aug 24 (2015), doi:10.5772/58655.
  - [15] For a review, see, e.g., T. P. Devereaux and R. Hackl, *Rev. Mod. Phys.* **79**, 175 (2007).
  - [16] J. Demsar, R. D. Averitt, A. J. Taylor, V. V. Kabanov, W. N. Kang, H. J. Kim, E. M. Choi, and S. I. Lee, *Phys. Rev. Lett.* **91**, 267002 (2003).
  - [17] M. Beck, M. Klammer, S. Lang, P. Leiderer, V. V. Kabanov, G. N. Gol'tsman, and J. Demsar, *Phys. Rev. Lett.* **107**, 177007 (2011).
  - [18] R. Matsunaga and R. Shimano, *Phys. Rev. Lett.* **109**, 187002 (2012).
  - [19] L. Luo, I. Chatzakis, A. Patz, and J. Wang, *Phys. Rev. Lett.* **114**, 107402 (2015).
  - [20] L. Luo, X. Yang, X. Liu, Z. Liu, C. Vaswani, D. Cheng, M. Mootz, X. Zhao, Y. Yao, C.-Z. Wang, K.-M. Ho, I. E. Perakis, M. Dobrowolska, J. K. Furdyna, and J. Wang, *Nat. Commun.* **10**, 607 (2019).
  - [21] T. Mori, E. J. Nicol, S. Shiizuka, K. Kuniyasu, T. Nojima, N. Toyota, and J. P. Carbotte, *Phys. Rev. B* **77**, 174515 (2008).
  - [22] X. Yang, C. Vaswani, C. Sundahl, M. Mootz, L. Luo, J. H. Kang, I. E. Perakis, C. B. Eom, and J. Wang (unpublished).
  - [23] J. S. Kim, G. N. Tam, and G. R. Stewart, *Phys. Rev. B* **92**, 224509 (2015).
  - [24] C. S. Owen and D. J. Scalapino, *Phys. Rev. Lett.* **28**, 1559 (1972).
  - [25] V. V. Kabanov, J. Demsar, and D. Mihailovic, *Phys. Rev. Lett.* **95**, 147002 (2005).
  - [26] A. Rothwarf and B. N. Taylor, *Phys. Rev. Lett.* **19**, 27 (1967).
  - [27] See Supplemental Material at <http://link.aps.org/supplemental/10.1103/PhysRevB.99.094504> for more information about materials, methods and further discussions. The Supplemental Material contains Refs. [33–44].

- [28] E. L. Wolf, J. Zasadzinski, G. B. Arnold, D. F. Moore, J. M. Rowell, and M. R. Beasley, *Phys. Rev. B* **22**, 1214 (1980).
- [29] X. Yang, L. Luo, M. Mootz, A. Patz, S. L. Bud'ko, P. C. Canfield, I. E. Perakis, and J. Wang, *Phys. Rev. Lett.* **121**, 267001 (2018).
- [30] A. Patz, T. Li, L. Luo, X. Yang, S. Bud'ko, P. C. Canfield, I. E. Perakis, and J. Wang, *Phys. Rev. B* **95**, 165122 (2017); A. Patz, T. Li, X. Liu, J. K. Furdyna, and I. E. Perakis, and J. Wang, *ibid.* **91**, 155108 (2015).
- [31] P. C. Lingos, A. Patz, T. Li, G. D. Barmparis, A. Keliri, M. D. Kapetanakis, L. Li, J. Yan, J. Wang, and I. E. Perakis, *Phys. Rev. B* **95**, 224432 (2017).
- [32] J. Wang, G. A. Khodaparast, J. Kono, T. Slupinski, A. Oiwa, and H. Munekata, *Physica E (Amsterdam, Neth.)* **20**, 412 (2004).
- [33] D. C. Mattis, and J. Bardeen, *Phys. Rev.* **111**, 412 (1958).
- [34] J. Demsar, R. Averitt, A. Taylor, W. Kang, H. Kim, E. Choi and, S. Lee, *Int. J. Mod. Phys. B* **17**, 3675 (2003).
- [35] M. Perpeet, M. Hein, G. Müller, H. Piel, J. Pouryamout, and W. Diete, *J. Appl. Phys.* **82**, 5021 (1997).
- [36] T. P. Orlando, E. J. McNiff, Jr., S. Foner, and M. R. Beasley, *Phys. Rev. B* **19**, 4545 (1979).
- [37] R. A. Kaindl, M. C. Carnahan, J. Orenstein, D. S. Chemla, H. M. Christen, H.-Y. Zhai, M. Paranthaman, and D. H. Lowndes, *Phys. Rev. Lett.* **88**, 027003 (2001).
- [38] S. A. Kuzmichev, T. E. Kuzmicheva, and S. N. Tchesnokov, *JETP Lett.* **99**, 295 (2014); I. Mazin and V. P. Antropov, *Physica C (Amsterdam, Neth.)* **385**, 49 (2003).
- [39] W. Weber, *Phys. Rev. B* **8**, 5082 (1973); U. Haufe, G. Kerker, and K. H. Bennemann, *Solid State Commun.* **17**, 321 (1975).
- [40] J. Kortus, I. I. Mazin, K. D. Belashchenko, V. P. Antropov, and L. L. Boyer, *Phys. Rev. Lett.* **86**, 4656 (2001); B. Z. Xu and S. P. Beckman, *2D Mater.* **3**, 031003 (2016).
- [41] R. Zhang, P. Gao, X. Wang, and Y. Zhou, *AIP Adv.* **5**, 107233 (2015).
- [42] S. L. Budko, G. Lapertot, C. Petrovic, C. E. Cunningham, N. Anderson, and P. C. Canfield, *Phys. Rev. Lett.* **86**, 1877 (2001).
- [43] X.-J. Chen, V. V. Struzhkin, S. Kung, H.-k. Mao, R. J. Hemley, and A. N. Christensen, *Phys. Rev. B* **70**, 014501 (2004).
- [44] L. J. Vieland and A. W. Wicklund, *Phys. Rev.* **166**, 424 (1968); A. Junod, T. Jarlborg, and J. Muller, *Phys. Rev. B* **27**, 1568 (1983).